# Decline and partial rebound of the Labrador Current 1993-2004: Monitoring ocean currents from altimetric and CTD data

Guoqi Han[1], Kyoko Ohashi[1], Nancy Chen[1], Paul G. Myers[2]

Nuno Nunes[3], and Jürgen Fischer[3]

[1]Fisheries and Oceans Canada

Northwest Atlantic Fisheries Centre

St. John's, NL, A1C 5X1 Canada

[2]Department of Earth & Atmospheric Sciences

University of Alberta

Edmonton, Alberta, T6G 2E3 Canada

[3]Leibniz Institute of Marine Sciences (IFM-GEOMAR), Kiel, Germany

August 8, 2010

(Revised Version)

**ABSTRACT**

Monitoring and understanding of Labrador Current variability is important because it is intimately linked to the meridional overturning circulation and the marine ecosystem off northeast North America. Nevertheless, knowledge of its decadal variability is inadequate because of scarcity of current meter data. By using a novel synthesis of satellite altimetry with conductivity-temperature-depth (CTD) data we assess the Labrador Current variability north of the Hamilton Bank ($56^{o}$N) over 1993-2004. Our analysis shows a decline of the surface-to-bottom transport of current by 6.3 ± 1.5 Sv (1 Sv =$10^{6}$ $m^{3}$ $s^{-1}$) in the 1990s (significant at the 99% confidence level) and a likely partial rebound of 3.2 ± 1.7 Sv in the early 2000s (significant at the 89% confidence level only). The inferred multiyear changes in the Labrador Current transport seem to be primarily barotropic and positively correlated (at the 99% level) with the North Atlantic Oscillation at zero lag implying a fast response of the regional circulation to the atmospheric forcing variability. The results compare favorably with direct current measurements and recent model-based findings on the multi-year variability of the subpolar gyre and its underlying mechanisms. The study demonstrates the feasibility of combining altimetry and CTD data for assessing the climatic variability of the boundary currents.

## 1. Introduction

The subpolar Northwest Atlantic is a region of intense interaction between ocean and atmosphere. In particular, the wintertime convection in the Labrador Sea, resulting from extreme cold and dry winds, is an important process for intermediate water (Labrador Sea Water) formation (Clarke and Gascard, 1983). The deep Labrador Current, as part of the subpolar gyre, carries the Labrador Sea Water and other deep water masses equatorward along the Labrador Slope (Fig. 1). Further south off Newfoundland, there is prominent cross-slope exchange between the colder and fresher Labrador Current along the 1000-m isobath and the warmer and saltier North Atlantic Current which overpasses the Deep Western Boundary Current along the 4000-m isobath (Han et al., 2008; Bower et al., 2009). Studies (e.g. Han and Tang, 2001; Häkkinen and Rhines, 2004) have indicated that the North Atlantic subpolar gyre is closely related to the atmospheric variability in the North Atlantic, whose dominant mode is the well-known North Atlantic Oscillation (NAO) (Hurrell, 1995). However, a recent model study suggests that the weakening of the subpolar gyre in 1996 is a combined consequence of the atmospheric forcing change and the ocean state change in response to the persistently strong positive NAO state from 1989 to 1995 (Lohmann et al., 2009).

The advent of precise satellite altimetry in the 1990s provides new opportunities for the study of the Labrador Current and the Labrador Sea circulation (e.g. Han and Ikeda, 1996; Brandt et al., 2004; Häkkinen and Cavalieri, 2005). Using the TOPEX/Poseidon (T/P) and Geosat altimeter data, Han and Ikeda (1996) found the predominance of the steric height effect over the wind-driven barotropic response in the deep Labrador Sea on the seasonal scale. Han and Tang (1999) used T/P altimeter observations, concurrent wind data, and historical hydrographic measurements to study the seasonal cycle of velocity and transport in the Labrador Current and found a transport range of 10 Sv at the Hamilton Bank section. The transport was largest in winter and smallest in spring. Han

and Tang (2001) by combining the T/P data with the WOCE (World Ocean Circulation Experiment) density data obtained an interannual range of 6 Sv for the spring/summer transport from 1993 to 1998, and found a positive correlation between the transport variability and the fall/winter North Atlantic Oscillation. A subsequent study of Häkkinen and Rhines (2004) found declining subpolar circulation in the 1990s from satellite data and moored measurements. They suggested the decline was related to local buoyancy forcing instead of wind forcing. Nevertheless, Böning et al. (2006), using an ocean general circulation model, showed that the interannual variability of the Labrador Sea circulation was forced by both the heat flux and wind stress variability on the interannual scale. Biastoch et al. (2008) then showed that, at least in a non-eddy resolving model, that the wind and buoyancy variability interacted in an almost linear manner to drive the total variability. However, examining current meter records from 56$^{o}$N and 53$^{o}$N, Dengler et al. (2006) reported a systematic increase of the deep Labrador Current from the late 1990s to the early 2000s. Most recently, Sarafanov et al. (2010), by combining altimetry and hydrography, inferred an intensification of the western boundary current at the intermediate and deep levels at Cape Farewell between the mid-1990s (1994-1997) and 2000s (2000-2007).

In this paper, we synthesize satellite altimetry sea surface height observations with CTD data to calculate the total geostrophic current and to study the variability in the Labrador Current from 1993 to 2004, providing insights into the multi-year variability of the Labrador Current from a novel perspective of satellite and CTD observations.

## 2. Data and Methods

### 2.1 Altimetric data

We use weekly merged sea surface height anomalies from AVISO, which are an objectively mapped product of TOPEX/Poseidon/Jason-1, ERS-1, ERS-2, Geosat-Follow-on and Envisat along-track altimeter data, with a 1/4$^o$ Mercator projection grid (Ducet at al. 2000). The zonal and meridional spacing for each grid is identical and varies with the latitude. Therefore the spatial resolution increases with latitude. All standard corrections were made to the along-track data to account for atmospheric (wet troposphere, dry troposphere, and ionosphere delays) and oceanographic (electromagnetic bias; ocean, load, solid Earth and pole tides) effects. Adjustments were made to ensure data consistency among different missions (Ducet et al. 2000).

In the western Labrador Sea around 55$^o$N, the along-track data were low-pass smoothed with a cut-off scale of 70 km and the mapping correlation scale is about 150 km (Ducet et al., 2000). Sea level anomalies have a root mean square error of 2-3 cm. We use the data offshore of the 600-m isobath from April to September (see 2.4), therefore the data quality degradation associated with coastal regions and ice presence is not an issue here.

**2.2 Hydrographic data**

Water density is computed from CTD data on WOCE's AR7W section across the Labrador Sea (see Fig.1 for location). The AR7W section is one of WOCE's repeat hydrographic sections, which has been occupied by the Bedford Institute of Oceanography every spring/summer since 1990 (The Labrador Sea Group, 1998; the data for 2000-2004 were provided by Allyn Clarke). We use the CTD data from 1993 to 2004, excluding 2000 when there was no data available inshore of 1100 m. In 1996 the section was also occupied in the fall, and CTD data from that cruise are used for error estimation. Table 1 presents the detailed information on the date of data collection and the number of stations used in this study.

**2.3 Wind velocity data**

Wind velocity data compiled by the U.S. National Climatic Data Center (NCDC) are used to calculate wind stress curls over the North Atlantic during the period 1993-2004. The wind velocity data are available over a $0.25^o$ global grid, and data with a temporal resolution of six hours (the finest available) are used. Wind speeds are a blend of observations from up to six satellites, and wind directions were derived by NCDC from the National Center for Environmental Prediction (NCEP) Reanalysis 2 data. During winter and spring the wind data are often not available off Labrador and Greenland due to the presence of sea ice.

**2.4 Calculation of geostrophic currents and transport**

The calculation of the sea surface current and volume transport is based on the geostrophic and hydrostatic equations, given by

$$fv = -\frac{1}{\rho_0}\frac{\partial p}{\partial x} \tag{1}$$

$$p = g\,\rho_0\zeta + g\int_z^0 \rho dz \tag{2}$$

where $x$ is the horizontal coordinate along a cross-shelf transect positive offshore (e.g. the AR7W transect, Fig. 1), $f$ is the Coriolis parameter, $p$ is the pressure, $v$ is the geostrophic velocity perpendicular to the transect (positive equatorward), $z$ is the vertical coordinate positive upward with $z$=0 at the mean sea level, $g$ is the gravitational acceleration, $\rho$ is the density of water, $\rho_0$ is the reference density, and $\zeta$ is the altimetric sea surface height referenced to an ocean geoid and corrected for atmospheric and oceanic effects. Note that the wind-driven Ekman transport is not

included here, since it is negligible in the Labrador Current transport and variability (Han and Tang, 2001).

The surface geostrophic current is determined solely by sea surface slope:

$$v(x) = -\frac{g}{f}\frac{\partial \zeta}{\partial x} \tag{3}$$

The geostrophic current at any depth $z$ is given by

$$v(x,z) = -\frac{g}{f}\frac{\partial \zeta}{\partial x} + \frac{g}{\rho_o f}\int_0^z \frac{\partial \rho}{\partial x} dz \tag{4}$$

In the conventional geostrophic calculation, one assumes a level of no motion to determine the sea level $\zeta$ from Eq. (4). Then the geostrophic current at any location can be determined from the sea level gradient and density gradient in the horizontal. But the assumed level of no motion is subject to large uncertainty and can be significantly unrealistic, for example, for the Antarctic Circumpolar Current (Tapley et al., 2003) and the Labrador Current (Han and Tang, 2001; Fischer et al., 2004). In a recent study by Kieke and Rhein (2006) a reference level at 1400 dbar was used to assess the decadal variability of the dense part of the Labrador Current north of Hamilton Bank. Such estimates do not take into account the variability of the alongshore velocity at the reference level on a decadal time scale. The short-term to decadal variability can be considerable at the intermediate depths in the western boundary current system, as discussed, e.g., by Sarafanov et al. (2010). In the present geostrophic calculation, the use of the sea surface as the reference level along with the satellite altimetry data providing information on the sea-surface reference currents in principle eliminates this problem.

Integrating Eq. (1) over depth and neglecting the bottom boundary layer, we obtain the depth-averaged current $V$:

$$V(x) = -\frac{g}{f}\frac{\partial \zeta}{\partial x} - \frac{1}{f}\int_{-H}^{0}\frac{\partial b}{\partial x}dz - \frac{1}{Hf}\int_{-H}^{0} z\frac{\partial b}{\partial x}dz \quad (5)$$

$$b = \frac{g}{\rho_0}[\rho(x,z) - \overline{\rho}(z)] \quad (6)$$

where $H$ is the local water depth, $b$ is the buoyancy parameter, and $\overline{\rho}(z)$ is a reference density obtained by averaging ρ at a given depth across the transect.

The cumulative volume transport $T$ from $x_1$ to $x_2$ is given by

$$T = -\frac{g}{f}\int_{x_1}^{x_2}\frac{\partial \zeta}{\partial x}Hdx - \frac{1}{f}\int_{x_1}^{x_2} H\int_{-H}^{0}\frac{\partial b}{\partial x}dzdx - \frac{1}{f}\int_{x_1}^{x_2}\int_{-H}^{0} z\frac{\partial b}{\partial x}dzdx \quad (7)$$

To bypass the error associated with the marine geoid, we will consider the transport anomalies only in the present study. For the transport anomaly, one can use the anomalies of the sea surface height and buoyancy parameter in Eq. (7).

From Eq. (7) the total cumulative transport anomalies are calculated from concurrent altimetric and CTD density data in 1993-2004, except 2000. Given the high-frequency spatial and temporal variability of the Labrador Current and the availability of altimetry and CTD data, we use the merged and gridded altimetry data averaged from spring to summer (April – September) and interpolated onto the locations of CTD stations (Fig. 2). Instantaneous CTD data are used as proxy, with a mean duration of about 5 days and a collection period spanning from May to July (late spring to early summer) depending on the year (Table 1). Dengler et al.'s (2006) current measurements for 1996-2005 suggest that the 3400-m isobath is approximately the boundary separating the southward deep Labrador Current from the northward recirculation in the surface and intermediate (Labrador Sea Water) levels. Therefore we choose to integrate from the 600-m isobath to 3400-m isobath as the baseline case. A small fraction of the transport at the edge of the Labrador Current

(recirculation) may be excluded (included) in individual years, but for multi-year averages this is a robust choice of boundary.

The error in the present calculation of the seasonal mean transport anomalies is mainly associated with the altimetry measurements of the sea surface height anomalies and the use of the instantaneous density as the proxy for the seasonal mean, as discussed by Han and Tang (2001). Their analysis indicates that the error in the first term when integrated from the shelf-edge to the deepest Labrador Sea (3600 m) is about 2 Sv, associated with altimetric measurement and correction errors, and that the mismatch of the time period may induce an error of 2.5 Sv in the second term of Eq. (7), while the mismatch-induced error in the third term is negligible.

In the present study we take a more comprehensive approach to assess transport uncertainties. First, for estimating the uncertainty associated with the altimetry measurements of the sea surface height anomalies we replace the April-September mean sea level anomalies with weekly mean data to compute the weekly mean transport anomalies during the period each year. Standard errors can then be estimated from the differences of the weekly transport anomalies. Second, for estimating the uncertainty associated with the use of the instantaneous density one possible way is to calculate the difference by combining the mean altimetry profile with more than one CTD section in a given spring/summer period. Unfortunately only one CTD section is available for each spring/summer period as shown in Table 1. Nevertheless, there is an October CTD section in 1996. We replace the May CTD section with the October section. The resulting transport anomaly difference is 7.5 Sv. When we account for the seasonal change of ~5 Sv from spring to fall (Han and Tang, 1999), the difference is 2.5 Sv. If we assume the errors are independent in the two calculations, the uncertainty as a result of the use of the instantaneous CTD section is estimated to be 1.8 Sv. Further, we use April to September climatological monthly-mean density sections to

replace WOCE CTD sections. The climatological density sections are obtained by interpolating Geshelin et al.'s (1999) $1/6^o$ by $1/6^o$ climatology. The standard deviations of the calculated transport anomalies vary from 1.3 Sv in 1994 to 1.7 Sv in 2001. In 1996 the standard deviation is 1.5 Sv, close to the estimate based on the May and October CTD sections. Therefore, we use the standard deviations based on the density climatology as a proxy for the transport uncertainties associated with the use of the instantaneous density. Third, we consider the uncertainties associated with the extrapolation in the bottom triangles based on Bacon's (1998) method. Finally, the root sum square of the estimates associated with the altimetric error, density proxy, and bottom triangle extrapolation are used as a proxy for the April-September mean transport anomalies each year.

Note that the standard deviations based on the density climatology should be same for all years. But the density climatology is interpolated onto the WOCE CTD cast locations during the calculation, which are different among years. Therefore, the differences of the calculated standard deviations among years represent additional uncertainties contributed by station spacing and bottom topography approximation.

An alternative way to estimate the total transport error is by comparing our results with estimates based on direct current measurements such as the Lowered acoustic Doppler current profiler (LADCP) data of Dengler et al. (2006). The $56^o$N transect of Dengler et al. (2006) is generally coincident with the AR7W CTD section in the western Labrador Sea. The LADCP measurement periods in a given year were usually one or two months later than those of the AR7W CTD observations. These are synoptic snapshots of both intraseasonal variability (10 – 30 day variability) and longer term variance of the boundary current, and thus, large variability between individual realizations should be expected.

**3. Results**

We will focus our analysis on the Labrador Current transport anomalies across the WOCE AR7W line between the 600- and 3400-m isobaths, based on the merged altimetry and hydrographic data. A timeseries of the total transport anomalies is given in Figure 3a. Three distinct periods are observed. Between 1993 and 1995, the Labrador Current transport is strong (positive anomaly) and slowly decreasing. There is then a dramatic weakening in 1996, leading to a two-year period (1996-97) with significantly below-average transports (Fig. 3a). The rapid decline is associated with a period when both the winter deep convection and the wind stress curl associated with the Icelandic Low were extremely weak (Fig. 4). Finally, beginning in 1998 the transport slowly rebounds, leading to very small anomalies in 2002-2003 and a positive transport anomaly in 2004. The average transport anomalies are 3.4 Sv for 1993-1995, -2.9 Sv for 1996-1999 and 0.3 Sv for 2001-2004, respectively. As a result, the transport decreased by 6.3 Sv from the early to late 1990s and increased by 3.2 Sv from the late 1990s to the early 2000s.

The changes of transport are in good agreement with estimates by Dengler et al. (2006), and consistent with model and observational studies (Böning et al., 2006; Sarafanov et al; 2010). Dengler et al. (2006) reported an increase of the deep Labrador Current by 5.8 Sv from the late 1990s (1996-1999) to the early 2000s (2001-2005) based on the LADCP measurements at the AR7W section in the western Labrador Sea. In addition, Böning et al.'s (2006) ocean general circulation simulations showed that the Labrador Sea circulation had a decline of ~8 Sv in the 1990s and a recovery of ~5 Sv from 1999 to 2003. The present estimates also seem to be qualitatively consistent with Fischer et al.'s (2004) results that the deep Labrador Current transport decreased until winter 1998/1999 and increased afterwards at the 53$^{o}$N transect. The increase of transport at this transect was estimated to be 8.7 Sv from late 1990s to the early 2000s (Dengler at

al., 2006). There is clear positive correlation between the Labrador Current variability and the winter NAO index (Fig. 3c), confirming Han and Tang's (2001) finding based on data covering a much shorter period. The correlation coefficient is 0.74 at the zero lag, statistically significant at the 99% confidence level.

From the uncertainties associated with the individual transport anomalies (Fig. 3a), the decline from 1995 to 1996 is significant at the 95% confidence level among all the consecutive year-to-year differences. The comparison between the LADCP and the altimetry/CTD transport anomalies shows large differences (Fig. 5). The RMS difference between the LADCP and the altimetry/CTD transport anomalies is calculated to be 4.6 Sv. Such a large difference is not surprising and presumably caused by intra-seasonal and recirculation variability (Dengler at al., 2006) and the fact that the LADCP and AR7W CTD measurement periods are not synoptic with regard to the intraseasonal fluctuations. In addition, LADCP station spacing was barely adequate to fully the resolve mesoscale eddy variability, and thus considerably, contributes to LADCP transport uncertainties when calculated from individual sections. Based on the above RMS difference, the RMS transport error is estimated to be 3.2 Sv.

The standard errors associated with the three mean transport anomalies are estimated to be 1.0, 1.1 and 1.2 Sv, respectively (Fig. 5). The earlier transport decrease of 6.3 Sv has a standard error of 1.5 Sv and is statistically significant at the 99% confidence level, but the later transport increase of 3.2 Sv is significant at the 89% confidence level only, with a standard error of 1.7 Sv.

To show the sensitivity of the estimated transport anomaly to the offshore extent or the transport variability of the Labrador Sea gyre, we have calculated the cumulative transport anomaly from the 600-m isobath to a location 50 km offshore (east) of the 3400-m isobath. The variability of the transport anomalies shows generally similar features (Fig. 3b). Large differences are only seen

in 1996 and 2003, probably related to the strength and location of the counter-current in those years. The zero-lag correlation coefficient with the NAO index is 0.53, statistically significant at the 90% confidence level. The transport decrease from the early and late 1990s is 4.7 Sv, significantly different from zero at the 90% confidence level, while the increase of 2.0 Sv from the late 1990s to the early 2000s is not significant at the 90% confidence level.

**4. Discussion**

The degree of the multi-year transport change can be measured by comparing the present estimates with the mean transport carried by the Labrador Current. Dengler et al. (2006) based on LADCP measurements showed the mean transport of the Labrador Current to be 30 Sv. Relative to Dengler's (2006) mean, the change in the mid-1990s represents a 25% decline. The change from the late 1990s to the early 2000s represents a 10% rebound.

The effect of local buoyancy forcing had been related to the decline of the subpolar gyre in the 1990s (Häkkinen and Rhines, 2004). The weakened net heat loss in winter 1996 (see Fig. 5B and 5C of Häkkinen and Rhines (2004)) essentially shut down the deep convection and flattened the isopycnal dome that is present in the western Labrador Sea in normal convection years, which resulted in the decrease of the Labrador Current. On the other hand, the ocean interior also responds to the wind stress variability barotropically and/or baroclinically and to the baroclinic overflow variability (the Denmark Strait Overflow). The Labrador Sea circulation is closely linked to the wind stress curl associated with the Icelandic Low (Han and Tang, 2001). As the NAO-related atmospheric forcing weakens, the reduced cyclonic wind stress curl associated with the Icelandic Low could reduce the subpolar gyre (Fig. 4). The zero-lag correlation between the cyclonic wind stress curl and the Labrador Current transport is 0.48, significant at the 85% confidence level only.

While the baroclinic response of the subpolar gyre to the wind stress variability may take several years, the barotropic response is much more rapid (Häkkinen and Rhines, 2004; Han, 2005). Our analysis indicates that the total Labrador Current transport has a positive correlation with the NAO index at essentially zero lag (Fig. 3), suggesting a fast oceanic response of a predominantly barotropic nature.

To provide further indication of the barotropic response, we have examined the transport variability for each of four layers in the western Labrador Sea. They are the Labrador Sea Surface Water (potential density <27.7 kg/m$^3$), a broad intermediate water layer encompassing various mode waters ranging from Irminger Water to classical Labrador Sea Water (27.7~27.8 kg/m$^3$), and two components of the North Atlantic Deep Water, the Iceland-Scotland Overflow Water (ISOW, 27.8~27.88 kg/m$^3$), and the Denmark Strait Overflow Water (DSOW, >27.88 kg/m$^3$). The transport anomalies in all four layers have positive correlation with the winter NAO index at zero lag. However, only the correlation in the intermediate layer is significant at the 90% confidence level. The transports in all four layers generally decreased from the early 1990s to the late 1990s (Fig. 6), though only the decrease in the top layer is significant at the 95% confidence level. The decline started a year later in the DSOW layer while the transport in the mode water layer began to rebound rapidly post 1996. For this intermediate layer, although Dengler et al. (2006) found that the Labrador Current transport increased after 1999, Myers et al. (2007) found a significant increase in the transport of Irminger Water into the Labrador Sea at Cape Farewell from the mid-1990s onward. Considering the mean transport anomalies over the three periods defined previously, we can see that the transports recovered to some degree (though not significant at the 95% confidence level) from the late 1990s to the early 2000s except for the ISOW layer. Despite the striking differences between the transport variability in the layers, the barotropic nature of the long-term transport

variability can be seen in Figure 6 from a general similarity of the transport changes between the three consecutive periods.

In addition, Böning et al. (2006) using an ocean general circulation model showed that the transport of the Labrador Sea circulation declined by ~8 Sv in the 1990s and rebounded by ~5 Sv from 1999 to 2003. They also found that the former was related to variability in both the net heat flux and the wind stress, while the latter was related to the increase of the wind stress curl despite the low net heat flux and weak deep convection. The strong decline of the North Atlantic subpolar gyre in 1996 was further explained as the ocean state change after the persistently strong NAO forcing in 1989-1995 (Lohmann et al., 2009).

**5. Conclusions**

Multi-year variability of the Labrador Current volume transport has been studied using merged and along-track satellite altimetry data from AVISO and hydrographic data from a WOCE transect since the 1990s. Total geostrophic transport anomaly of the Labrador Current from altimetry and hydrography shows a notable decline in 1996 (6.3 ± 1.5 Sv, significant at the 99% confidence level) and a likely partial recovery (3.2 ± 1.5 Sv, significant at the 89% confidence level) in the early 2000s. This variability looks coherent through the water column except for the ISOW layer, which does not show the same rebound during the early 2000s. It is found that the Labrador Current variability is positively correlated (significant at the 99% confidence level) with the winter NAO index at the zero lag. The likely coherence in the vertical and the zero-lag correlation with NAO imply that the Labrador Current variability is primarily of barotropic nature. The present results are consistent with estimates based on in situ current measurements for the Labrador Current and recent model results (Böning et al., 2006) for the North Atlantic subpolar

gyre, demonstrating the feasibility of using altimetry and CTD data to monitor the climatic variability of the Labrador Current. This is an important result, because long-term current meter moorings are rare and expensive while this technique suggests a way for improved monitoring of important oceanic flows such as the Labrador Current. Without the altimetric data this would not be possible.

The present method can be applied to other major ocean current systems worldwide, e.g., the Antarctic Circumpolar Current which has significant deep flows and where again, the use of a level of no motion may not be appropriate. It points to the importance for field oceanographers to consider long-term monitoring transects along satellite ground tracks to achieve great synergy between satellite altimetry and CTD measurements. Nevertheless, one should bear in mind that the calculated transport may have large uncertainties associated with altimetric data errors and limited CTD data availability. Error analysis of the transport variability is often challenging because of limited CTD data availability, which may be made easier by coordinating field observations with satellite sampling.

## ACKNOWLEDGMENTS

The suggestions from the two anonymous reviewers and Dr. Frank Bryan helped improve the error analysis. This work is supported by: the ArcticNet, a Network of Centres of Excellence of Canada, the Canadian Space Agency Government Research Initiative Program, the Program for Energy Research and Development of Natural Resources Canada, and the German Ministry of Education and Research, BMBF.

**REFERENCES**

Bacon, S. (1998), Decadal variability in the outflow from the Nordic seas to the deep Atlantic Ocean, *Nature, 394*, 871-874.

Biastoch, A., C. Böning, J. Getzlaff, J.-M. Molines and G. Madec (2008), Causes of interannual-decadal variability in the meridional overturning circulation of the midlatitude North Atlantic Ocean, *Journal of Climate, 21*, 6599-6615.

Bower, A., M. Lozier, S. Gary, and C. Böning (2009), Interior pathways of the North Atlantic meridional overturning circulation, *Nature, 459 (7244),* 243-247 DOI: 10.1038/nature07979.

Böning, C., M. Scheinert, J. Dengg, A. Biastoch, and A. Funk (2006), Decadal variability of subpolar gyre transport and its reverberation in the North Atlantic overturning, *Geophys. Res. Lett.*, *33*, L21S01, doi:10.1029/2006GL026906.

Brandt P., F. A. Schott, A. Funk, and C. S. Martins (2004), Seasonal to interannual variability of the eddy field in the Labrador Sea from satellite altimetry, *J. Geophys. Res.*, *109*, C02028, doi:10.1029/2002JC001551.

Clarke, R.A., and J.C. Gascard (1983), The formation of Labrador Sea water. Part I: Large-scale processes, *J. Phys. Oceanogr.*, *13*, 1764-1778.

Dengler, M., J. Fischer, F.A. Schott and R. Zantopp (2006), Deep Labrador Current and its variability in 1996-2005, *Geophys. Res. Lett.*, *33*, L21S06, doi:10.1029/2006GL026702.

Ducet N., P.Y. Le Traon, and G. Reverdin (2000), Global high resolution mapping of ocean circulation from TOPEX/Poseidon and ERS-1 and -2, *J. Geophys. Res.*, *105*, 19477-19498.

Fischer, J., F.A. Schott and M. Dengler (2004), Boundary circulation at the exit of the Labrador Sea, *J. Phys. Oceanogr.*, *34*, 1548-1570.

Geshelin, Y., J. Sheng, and R.J. Greatbatch (1999), Monthly mean climatologies of temperature and salinity in the western North Atlantic, *Can. Tech. Rep. Hydrogr. Ocean Sci. 153*, 62pp.

Häkkinen, S. and P.B. Rhines (2004), Decline of subpolar North Atlantic circulation during the 1990s, *Science*, *304*, 555-559.

Häkkinen S., and D. J. Cavalieri (2005), Sea ice drift and its relationship to altimetry-derived ocean currents in the Labrador Sea, *Geophys. Res. Lett.*, *32*, L11609, doi:10.1029/2005GL022682.

Han G. (2005), Wind-driven barotropic circulation off Newfoundland and Labrador, *Continental Shelf Research*, *25*, 2084-2106.

Han, G. (2006), Low-frequency variability of sea level and currents off Newfoundland, *Advances in Space Research*, *38*, 2141-2161.

Han, G., and M. Ikeda (1996), Basin-scale variability in the Labrador Sea from TOPEX/Poseidon and Geosat altimeter data, *J. Geophys. Res.*, *101*, 28,325-28,334.

Han, G., and C.L. Tang (1999), Velocity and transport in the Labrador Current determined from altimetric, hydrographic and wind data, *J. Geophys. Res.*, *104*, 18,047-18,057.

Han, G., and C.L. Tang (2001), Interannual variations of volume transport in the western Labrador Sea based on TOPEX/Poseidon and WOCE data, *J. Phys. Oceanogr.*, *31*, 199-211.

Han G., Z. Lu, Z. Wang, J. Helbig, N. Chen, and B. deYoung (2008), Seasonal variability of the Labrador Current and shelf circulation off Newfoundland, *J. Geophys. Res.*, *113*, C10013, doi: 10.1029/2007JC004376.

Hurrell, J.W. (1995), Decadal trends in the North Atlantic Oscillation: regional temperatures and precipitation, *Science, 269*, 676-679.

Kieke, D., and M. Rhein (2006), Variability of the overflow water transport in the western subpolar North Atlantic, 1950-97, *J. Phys. Oceanogr.*, *36*, 435-456.

Lohmann, K., H. Drange, and M. Bentsen (2009), A possible mechanism for the strong weakening of the North Atlantic subpolar gyre in the mid-1990s, *Geophys. Res. Lett.*, *36*, L15602, doi:10.1029/2009GL039166.

Myers, P.G., N. Kulan and M.H. Ribergaard (2007), Irminger Water variability in the West Greenland Current, *Geophys. Res. Lett.*, *34*, doi:10.1029/2007GL030419

Pickart, R.S., and M. A. Spall (2007), Impact of Labrador Sea Convection on the North Atlantic Meridional Overturning Circulation, *J. Phys. Oceanogr.*, 37, 2207-2227.

Sarafanov A., A. Falina, P. Lherminier, H. Mercier, A. Sokov, and C. Gourcuff (2010), Assessing decadal changes in the Deep Western Boundary Current absolute transport southeast of Cape Farewell (Greenland) from hydrography and altimetry, *J. Geophys. Res.*, (in press).

Tapley B.D., D.P. Chambers, S. Bettadpur, and J.C. Ries (2003), Large scale ocean circulation from the GRACE GGM01 Geoid, *Geophys. Res. Lett.*, *30* (22):doi:10.1029/2003GL018622.

The Lab Sea Group (1998), The Labrador Sea deep convection experiment. *Bulletin of the American Meteorological Society*, *79*, 2033-2058.

Table 1. Number of AR7W CTD stations used in this study (between the Labrador Shelf and the deepest part of the Labrador Sea) and the dates they were occupied:

| Year | Date | No. of stations |
|---|---|---|
| 1993 | June 19 – 22 | 17 |
| 1994 | May 31 - June 5 | 24 |
| 1995 | June 11 – 14 | 16 |
| 1996 | May 18 – 22 | 18 |
| 1996 | October 20 - 26 | 18 |
| 1997 | May 23 – 28 | 12 |
| 1998 | June 26 - July 1 | 17 |
| 1999 | July 1 - July 5 | 16 |
| 2000 | - | - |
| 2001 | June 4 – June 7 | 15 |
| 2002 | July 2 – July 6 | 10 |
| 2003 | July 23 – July 26 | 18 |
| 2004 | May 20 – May 22 | 15 |

Figure Caption

Figure 1. Map showing the study area and major geographical and circulation features. The AR7W hydrographic section in the Labrador Sea is displayed. The two filled circles on the section are the onshore (600 m) and offshore (3400 m) extents for the baseline calculation. The 200-, 1000-, 2000-, 3000- and 4000-m isobaths (thin lines) are also shown.

Figure 2. Altimetric sea level anomalies averaged for April-September and associated standard errors (vertical bars) in (a) 1993, (b) 1997 and (c) 2003. The sea level anomalies are interpolated on to the mid-points between hydrographic stations. Also shown are the potential density (kg $m^{-3}$) patterns across the AR7W CTD section in early summer in (d) 1993, (e) 1997, and (f) 2003. The triangle depicts the location of the 3400-m isobath. The horizontal axis measures the distance from the 600-m isobath to the deepest part of the Labrador Sea.

Figure 3. The Labrador Current transport anomalies across WOCE AR7W transect in the western Labrador Sea. (a) Total transport anomalies and uncertainties (vertical bars) for the baseline calculation between the 600- and 3400-m isobaths from the merged altimetry and hydrographic data. (b) The total transport anomalies for the sensitivity case, integrated from the 600-m isobath to a location 50 km offshore of the 3400-m isobath. (c) The winter NAO index anomalies.

Figure 4. Wind stress curl variability in the North Atlantic. (a) The spatial pattern of the first-mode EOF (which accounts for 17% of the total variance). (b) The wind stress curl anomalies averaged for December-March for subpolar (thin) and subtropical (thick) regions, respectively.

Figure 5. The Labrador Current transport anomalies and associated standard errors (vertical bars) between the 600- and 3400-m isobaths in the western Labrador Sea, for the baseline calculation from the merged altimetry and hydrographic data (open circles) and for the LADCP measurements (crosses) of Dengler et al. (2006). The thick horizontal bars depict the average transport anomalies for the baseline case in 1993-1995, 1996-1999, and 2001-2004, respectively. The thin horizontal bars depict the average transport anomalies for the LADCP measurements in 1996-1999 and in 2001-2005, respectively.

Figure 6. The Labrador Current transport anomalies across WOCE AR7W transect in the western Labrador Sea, associated with (a) the Labrador Sea Surface Water (potential density <27.7 $kg/m^3$), (b) intermediate waters (27.7~27.8 $kg/m^3$), (c) the Iceland-Scotland Overflow Water (27.8~27.88 $kg/m^3$) and (d) the Denmark Strait Overflow Water (>27.88 $kg/m^3$). The horizontal bars depict the average transport anomalies in 1993-1995, 1996-1999, and 2001-2004, respectively.

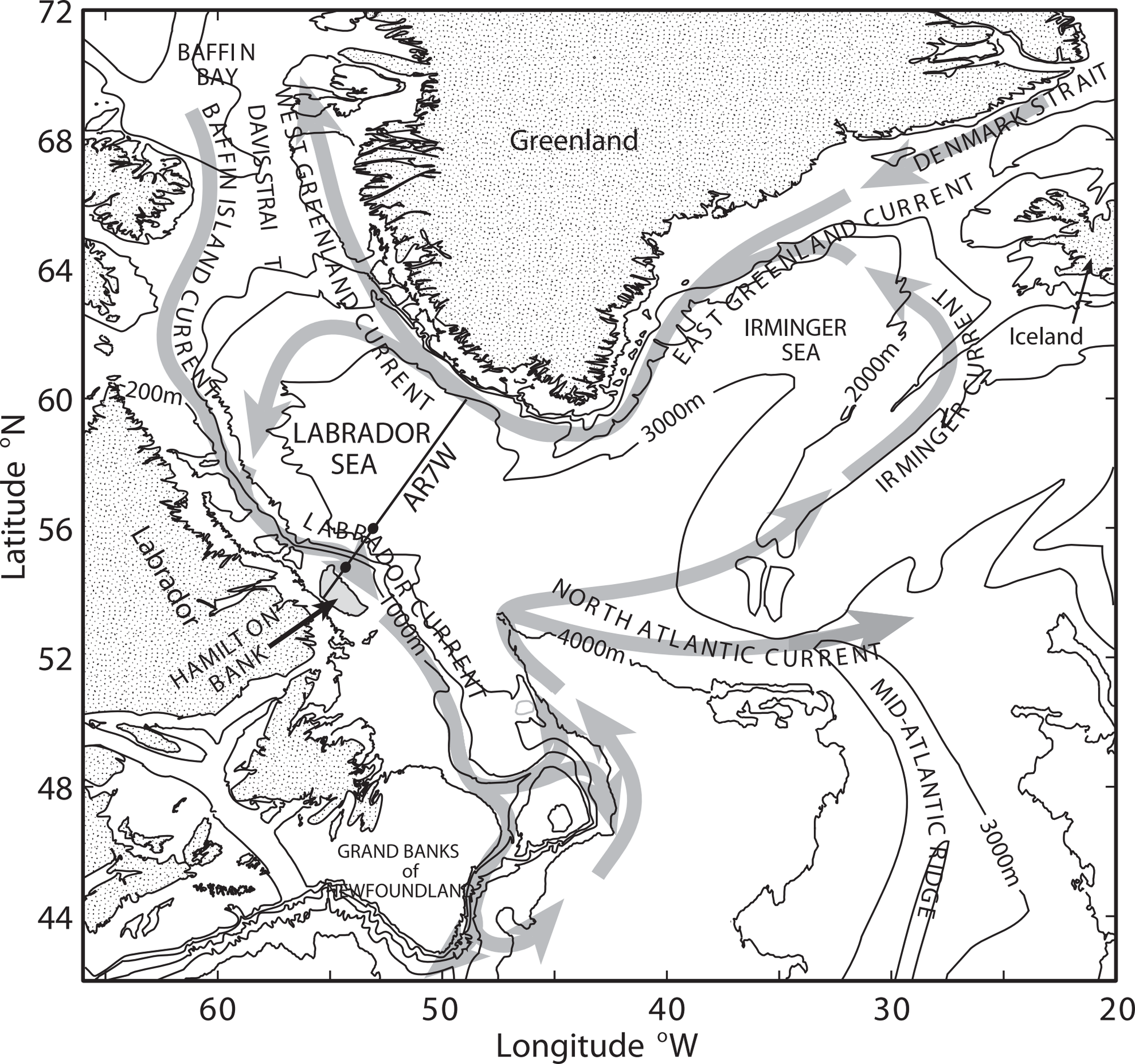
BAFFIN BAY
Greenland
DENMARK STRAIT
BAFFIN ISLAND CURRENT
WEST GREENLAND CURRENT
EAST GREENLAND CURRENT
IRMINGER SEA
Iceland
200m
3000m
2000m
LABRADOR SEA
AR7W
LABRADOR CURRENT
IRMINGER CURRENT
Labrador
HAMILTON BANK
1000m
NORTH ATLANTIC CURRENT
4000m
MID-ATLANTIC RIDGE
GRAND BANKS of NEWFOUNDLAND
Latitude °N
Longitude °W
72
68
64
60
56
52
48
44
60
50
40
30
20

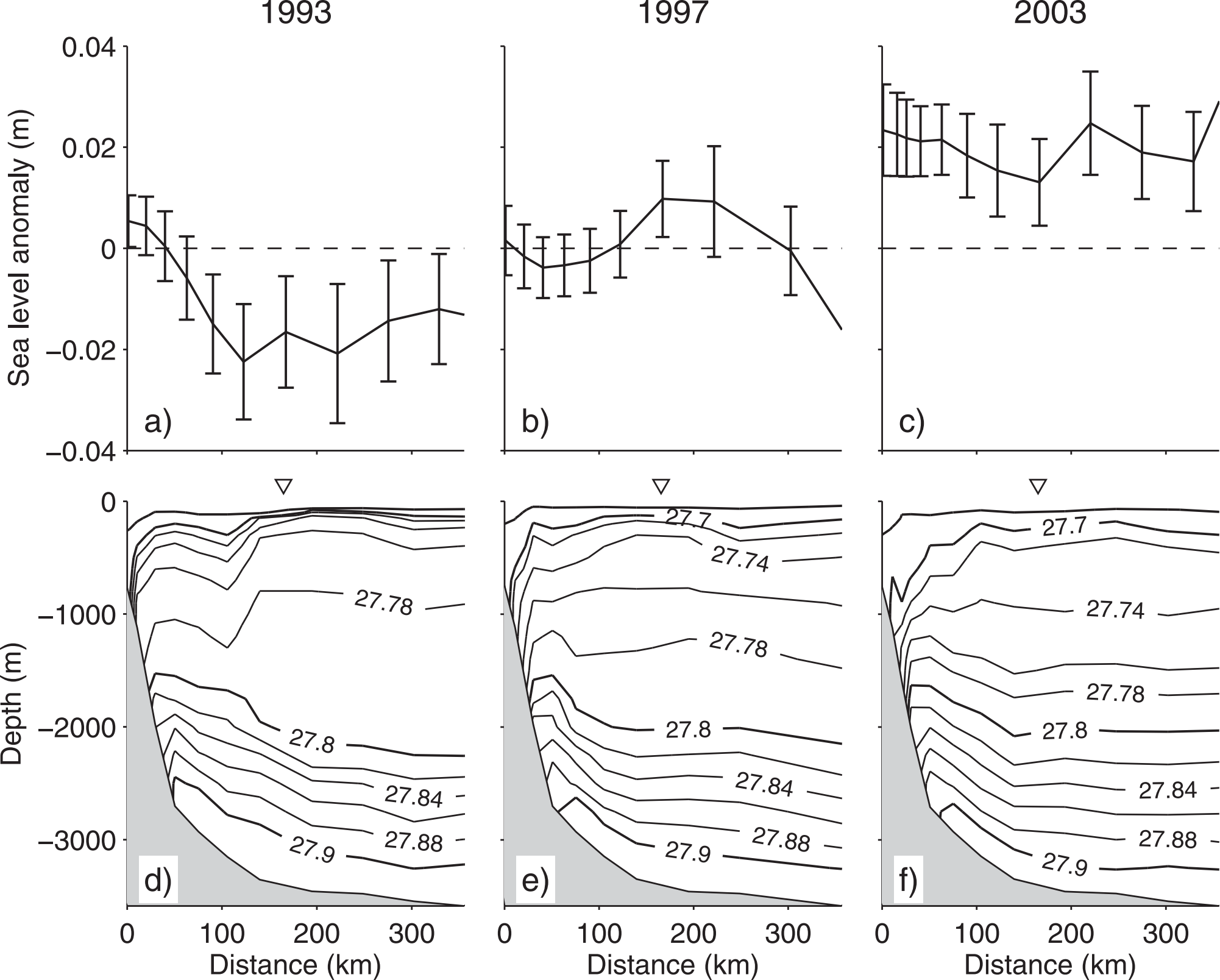
1993
1997
2003
Sea level anomaly (m)
0.04
0.02
0
−0.02
−0.04
a)
b)
c)
Depth (m)
0
−1000
−2000
−3000
27.7
27.74
27.78
27.8
27.84
27.88
27.9
d)
e)
f)
0
100
200
300
Distance (km)

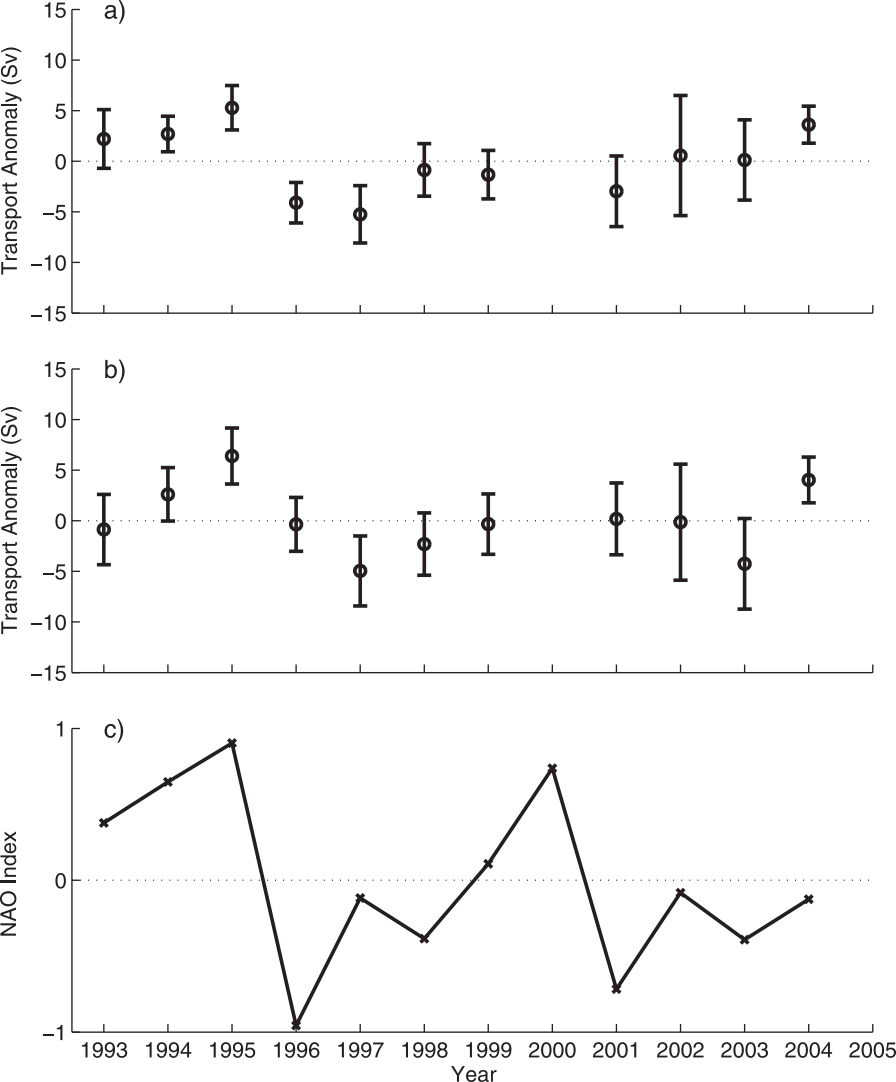
a)
b)
c)
Transport Anomaly (Sv)
NAO Index
Year
15
10
5
0
−5
−10
−15
1
−1
1993
1994
1995
1996
1997
1998
1999
2000
2001
2002
2003
2004
2005

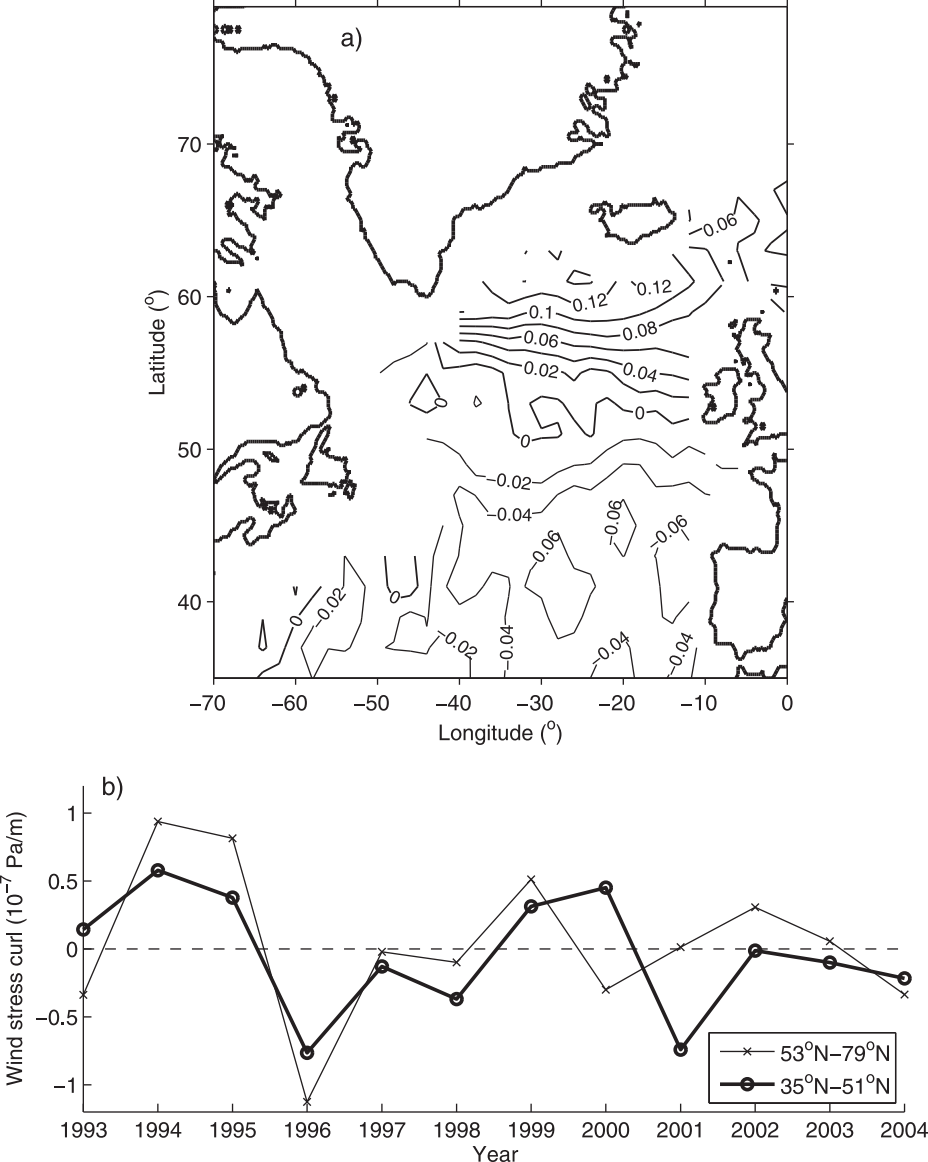
a)
Latitude (°)
Longitude (°)
70
60
50
40
−70
−60
−50
−40
−30
−20
−10
0
0.12
0.1
0.08
0.06
0.04
0.02
0
−0.02
−0.04
−0.06
b)
Wind stress curl ($10^{-7}$ Pa/m)
Year
1
0.5
0
−0.5
−1
1993
1994
1995
1996
1997
1998
1999
2000
2001
2002
2003
2004
53°N–79°N
35°N–51°N

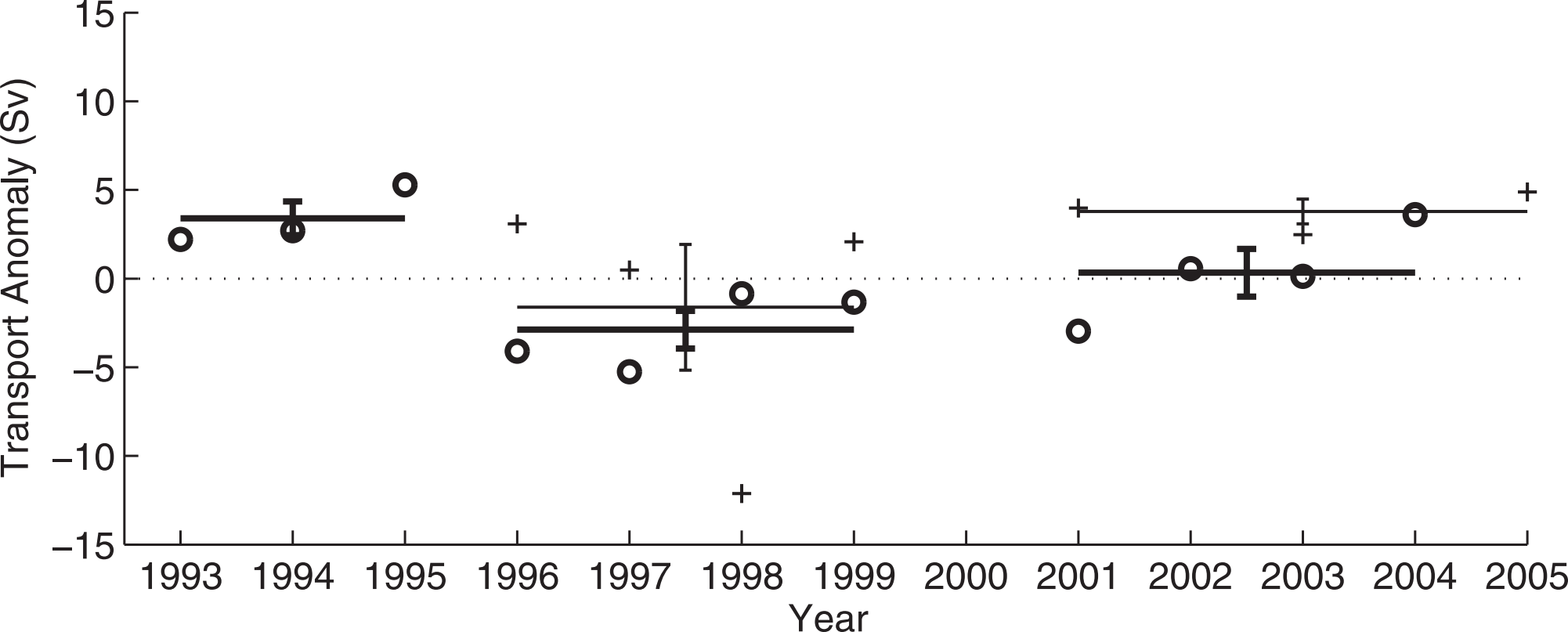
15
10
5
0
−5
−10
−15
Transport Anomaly (Sv)
1993
1994
1995
1996
1997
1998
1999
2000
2001
2002
2003
2004
2005
Year

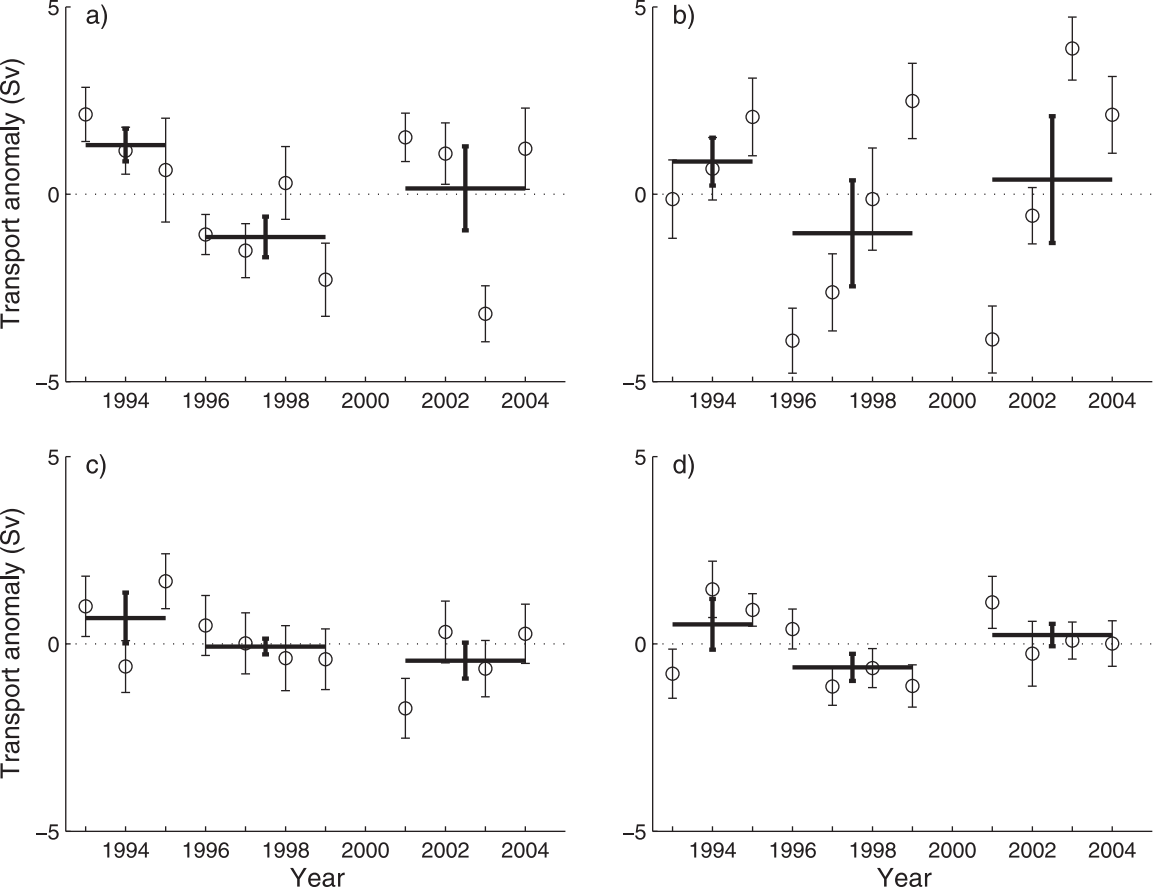
a)
b)
c)
d)
Transport anomaly (Sv)
Transport anomaly (Sv)
5
0
−5
1994
1996
1998
2000
2002
2004
Year
Year